Charge exchange neutral particle analysis with natural diamond detectors on LHD heliotron

M. Isobe[a] and M. Sasao
National Institute for Fusion Science, 322-6 Oroshi-cho, Toki-shi 509-5292 Japan

S. Iiduka
Department of Nuclear Engineering, School of Engineering, Nagoya University, Furo-cho, Chikusa-ku, Nagoya 464-8603 Japan

A. V. Krasilnikov
Troitsk Institute for Innovating and Fusion Research TRINITI, Troitsk, Moscow region, 142092, Russia

S. Murakami, T. Mutoh, M. Osakabe, S. Sudo, K. Kawahata, N. Ohyabu, O. Motojima, and LHD experiment group
National Institute for Fusion Science, 322-6 Oroshi-cho, Toki-shi 509-5292 Japan

(Presented on 19 June 2000)

Semiconductor detectors based on natural diamonds have been installed on the Large Helical Device (LHD) heliotron to measure the energy distribution of charge exchange fast neutral particles from different viewing angles. Advantages of a natural diamond detector (NDD) are (1) very compact size, (2) relatively easy handling, and (3) high energy resolution. Although NDDs are sensitive to visible light, vacuum ultraviolet, and soft x rays, unfavorable pulses produced by such radiation were greatly reduced by choosing an appropriate stainless steel shield in this experiment. In LHD, the time-resolved energy distribution of counter-going beam ions and ion cyclotron range of frequency-produced energetic ions have been successfully obtained by means of an NDD. The performance of NDDs as a neutral particle analyzer and its good suitability to LHD plasmas were demonstrated throughout this work. © *2001 American Institute of Physics.*
[DOI: 10.1063/1.1318250]

I. INTRODUCTION

Charge exchange neutral particle analyzers (NPA) have played an important role in diagnosing fast ion behavior in toroidal fusion plasmas because NPAs provide the energy distribution of fast ions. NPAs have been used to investigate not only energetic ion transport in neoclassical theory but also magnetohydrodynamic (MHD)-related phenomena, for instance, mode-fast particle resonances, effects of sawtooth activity on fast ion confinement, and so on.[1–6] These experimental studies have been so far carried out with a conventional NPA which consists of gas or foil stripping cell and energy and/or mass analyzers.

Recently, it was first reported by Krasilnikov that a solid state NPA based on natural diamond, which was developed in Troitsk Institute for Innovating and Fusion Research (TRINITI), Russia, was successfully operated on the Tokamak Fusion Test Reactor (TFTR) and it provided valuable information concerning energetic ion behavior in TFTR plasmas.[7] A solid state NPA is very attractive in its compact size and convenience compared to other NPA technologies. Another advantage is that a solid state NPA can give us more continuous data points in the energy spectrum of fast ions compared with a conventional NPA.

In this work, we employed two NDDs to diagnose the energy distribution of neutral beam (NB)-injected fast ions and ion cyclotron range of frequency (ICRF)-accelerated ions from different viewing angles in the Large Helical Device (LHD). Experimental results shown here were obtained in the second and third cycle of the LHD experiment. In Sec. II, the installation of NDDs on LHD and their electronics are described. In Sec. III, experimental results for energy distribution of NB ions and ICRF-produced energetic ions are reported. Orbits of energetic ions reaching NDD are also described in Sec. III. Finally, this work is briefly summarized in Sec. IV.

II. EXPERIMENTAL SETUP

LHD is a large superconducting fusion experiment device having major radius of 3.9 m and minor radius of 0.6 m.[8] The toroidal and poloidal periods are $m=10$ and $l=2$, respectively. Target plasmas are usually initiated by electron cyclotron resonance heating at 84 GHz. There are two negative ion source-based neutral beam injectors on LHD. Both injectors provide hydrogen beams and they are arranged for tangential injection in opposite directions, i.e., co- and counter (ctr.) direction. An ICRF heating system is also available in LHD.

The NDD has three layer structure, i.e., electrode-semiconductor (very pure natural diamond) electrode. The NDD employed in LHD is a specially developed detector having a very thin graphite front electrode, which makes it possible to detect low energy particles. Incident fast particles

[a]Electronic mail: isobe@nifs.ac.jp

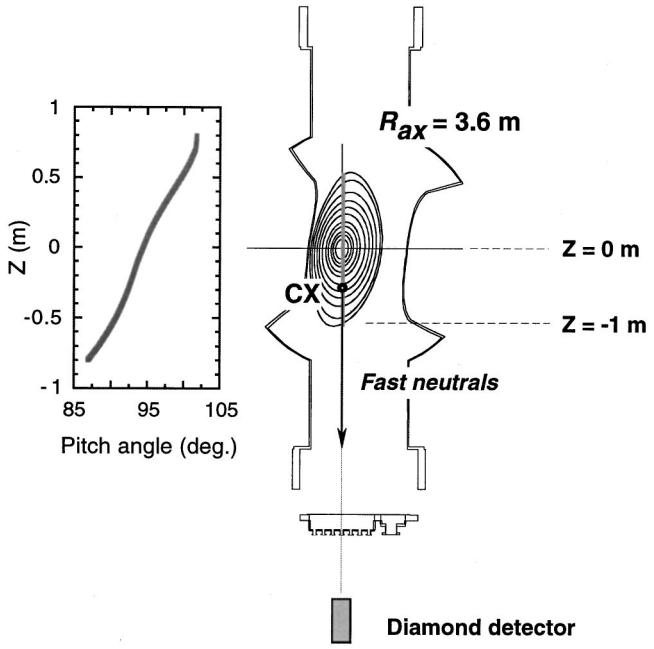

FIG. 1. Line of sight of the NDD on a perpendicular diagnostic port of LHD. The left figure shows the pitch angle distribution of fast particles detected by the NDD along the line of sight at $R_{ax}=3.6$ m.

produce electric charges inside the diamond. These charges are drawn by an externally applied bias voltage to the electrodes. A detailed description of an NDD is seen in Refs. 9 and 10.

The NDD is mounted inside a stainless steel cylinder of 30 cm length to shield the detector against vacuum ultraviolet (VUV) rays and soft x rays because the NDD is sensitive to such photon radiations. In order to view the plasma, we set a circular aperture having a fixed diameter of 1 mm on the opposite end, i.e., plasma side, of the cylinder. An additional aperture whose diameter can be changed is also installed 55 cm ahead of this fixed aperture to control the neutral particle flux coming into the NDD. Two NDDs are installed on LHD. One is installed on the equatorial plane with tangential line of sight to measure ctr.-going beam ions. The distance between the NDD and the magnetic axis position is about 8.3 m in this case. Another is set on a perpendicular diagnostic port to diagnose formation of energetic ion tail produced by ICRF. A line of sight of the NDD set on a perpendicular port is shown in Fig. 1. The position of the NDD is about 4.5 m below the magnetic axis position. The NDD is operated at room temperature in LHD. Because of sufficiently wide band gap (5.5 eV), it is not necessary to cool the detector to suppress thermal noise as long as we focus on detecting NB ions or ICRF-produced fast ions.

The electronic circuit employed here is shown in Fig. 2. The NDD was operated in pulse height analysis mode. The bias voltage was typically 100 V. The NDD was directly connected to a preamplifier (ORTEC-142A) to suppress electric noise as much as possible. The preamplifier was connected to a fast spectroscopic amplifier (CANBERRA-2024) by 2 m/50 Ω coaxial cable. The shaping time of the amplifier was always fixed to be the shortest value, 0.25 μs. Shaped output pulses were transferred from the torus hall to the diagnostics room with a 150 m/50 Ω coaxial cable. Pulse height distributions were analyzed on a system which consisted of an ultrafast analog to digital convertor (CANBERRA-8715) linked to a router and histgramming memory (TOYO-629). The sampling frequency was typically 100 Hz. Time-resolved PHA data from the NDD was stored in the LHD O2 database. The energy calibration was done by using a very thin ^{241}Am alpha spectrometry source of 15 nCi which is intended for calibrating solid state detectors. The energy resolution was also checked and it was estimated to be 8.7% with the same electronic circuits and coaxial cables used in the experiment. Test pulses with fixed voltage are continuously supplied to the test input of the preamplifier in order to monitor gain drift and the pile-up throughout this experiment.

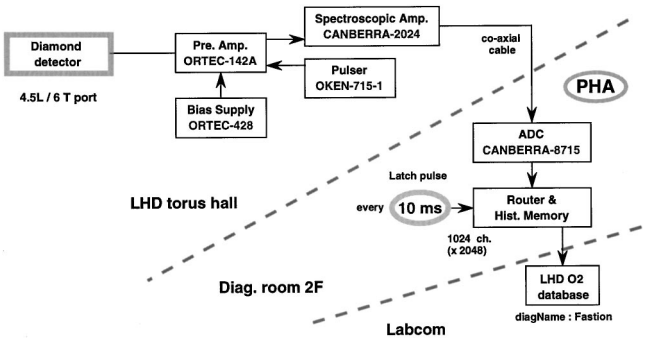

FIG. 2. Schematic drawing of the electronic circuit of the NDD.

III. MEASUREMENTS OF ENERGETIC ION DISTRIBUTION IN LHD

A. Counter-going beam ions

1. Experimental result

In LHD, time-resolved energy distributions of beam ions were successfully obtained by using NDDs. Figure 3 shows

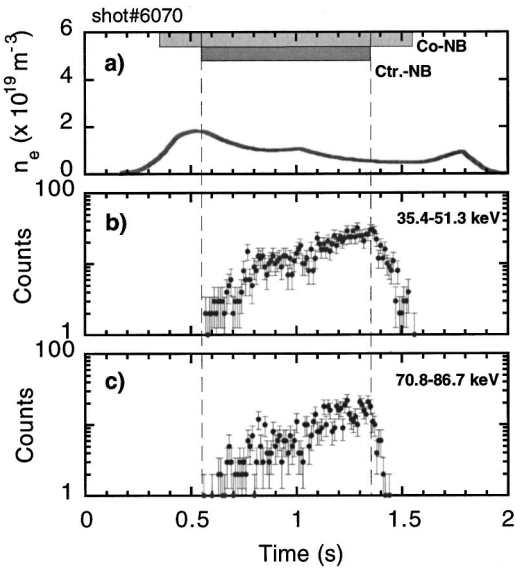

FIG. 3. Typical time traces of (a) n_e, (b) and (c) incoming flux of charge exchange fast neutral particles for counter-going beam ions. B_t and R_{ax} were 1.5 T and 3.75 m, respectively. Injection energy of ctr. NB was 101 keV.

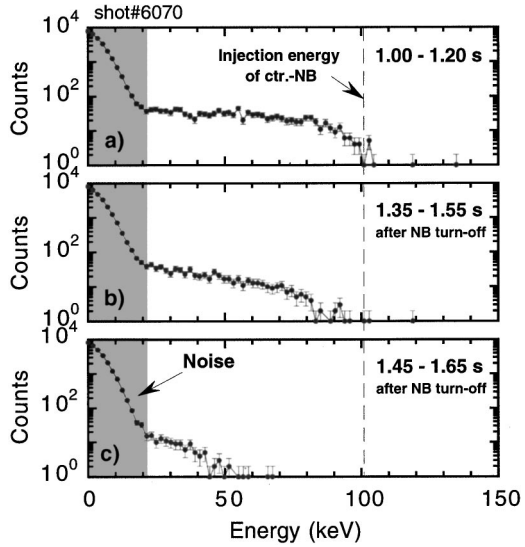

FIG. 4. Time behavior of the energy distribution of fast neutral particles for counter-going beam ions, (a) during NB, (b) and (c) after NB turn-off for the shot seen in Fig. 3. Signals in the low energy range (shaded area) are dominated by electric noise.

time traces of electron density, n_e, and fast neutral particle flux of ctr.-going beam ions for two different energy ranges. The toroidal magnetic field strength, B_t, and magnetic axis position, R_{ax}, were 1.5 T and 3.75 m, respectively. Ctr. NB was tangentially injected into a target plasma sustained by coinjected NB in this shot. The acceleration voltage of ctr.-injected NB was 101 kV. The NDD started to count pulses just after the ctr. NB was injected and the neutral particle flux gradually increased with time. It can be seen that the flux of lower energy particles decays slowly compared with that of higher energy particles after NB turn-off. This indicates deceleration of ctr.-going beam ions in the plasma. Figure 4 shows the energy spectra of ctr.-going beam ions for different times during the same shot as in Fig. 3. The maximum energy in the spectrum coincides with injection energy of ctr. NB [see Fig. 4(a)]. In the phase after the ctr.-injected NB turn-off, it may be clearly observed that the ctr.-going beam ions slow down with time [see Figs. 4(b) and 4(c)]. Signals seen in the low energy range (shaded area) are dominated by electric noise, which is mainly from the preamplifier. They also include pulses produced by low energy particles and photon radiation such as VUV rays and x rays. Therefore, interpretation of signals in the shaded area is rather complicated. In our system, the lowest detectable energy is about 20–30 keV, depending on electronic circuits, coaxial cables, external electromagnetic environment, and so on.

Generally, the neutral particle flux tends to decrease with increase of n_e. When n_e is above $3.0\times10^{19}\,\mathrm{m}^{-3}$, it is hard to detect neutral particles in the present system. This is probably due to strong attenuation of fast neutral flux along the line of sight of NDD. An interesting observation is that particle flux quickly disappears just after pellet injection. Another reason for loss of signal at high density may be the decrease of neutral density in a plasma with increasing n_e. If we install larger apertures, it may be possible to detect fast particles in high n_e plasmas. However, it is then expected that we will suffer pile-up in low n_e plasmas because of the increase of incoming fast neutrals. In order to overcome this problem, it is necessary to develop an ultrafast amplifier.

2. Orbit and transport

In order to see what type of fast ion orbits we observe, a full gyromotion following orbit code was developed. Orbits are calculated in the vacuum magnetic field in Cartesian coordinates. Energetic ions are launched on the line of sight with velocity vector toward the NDD and orbits are computed backward in time. The calculation shows that the NDD set on a tangential port detects ctr.-going transit particles. The NDD does not detect trapped beam ions in this viewing angle. The pitch angle of detected particles ranges from 140° to 180°.

The measured energy distribution of ctr.-going beam ions was compared with that predicted by the GNET code which simulates global neoclassical energetic ion transport incorporating the beam deposition calculation HFREYA. The GNET simulation reproduces well the measured energy distribution.[11] This suggests that neoclassical transport is important in understanding energetic ion behavior in LHD.

B. ICRF-accelerated protons

1. Experimental result

One ICRF experimental scenario in LHD is proton minority fundamental heating in He-majority plasmas.[12] Our objective is to diagnose the energy distribution of ICRF-accelerated protons in these LHD plasmas. Figure 5 shows time traces of n_e, W_p, T_e, neutral particle flux, and effective tail temperature $T_{\text{tail-eff}}$, taking into account the charge exchange (CX) process; $H^+ + He^0 \rightarrow H^0 + He^+$. The energy spectra of perpendicular tail ions are also shown in Fig. 5(e). The experimental parameters were; $B_t = 2.75\,\mathrm{T}$, $R_{ax} = 3.6\,\mathrm{m}$, and ICRF power $= 1.5\,\mathrm{MW}$ in this shot. It is clearly seen that ICRF starts to accelerate minority protons just after ICRH turn-on. After a while, the n_e and fast ion tail density reached the steady state. The energy of ICRF-accelerated protons goes up to 200–250 keV in the ICRF heating phase. It is seen that coinjected NB of 124 keV/0.6 MW increases T_e and the fast ion tail starts to grow further after NB turn-on. It seems that evolution of the fast ion tail follows the rise of T_e. After NB turn-off, the fast ion tail density returns to the previous level. The growth of the fast ion tail during NBI is inferred to be due to enhanced accumulation of energetic ions because of a longer slowing down time at higher T_e. We also observe a perpendicular component of beam ions in spite of tangential injection but the measured maximum energy is only about 70 keV. Therefore, the perpendicular component of beam ions is not a candidate to explain the growth of the fast ion tail while NB is injected. Analysis to check whether the growth of the fast ion tail due to increased T_e agrees with expectations from classical theory or not is now in process. In general, neutral particle flux increases with increasing n_e for the perpendicular detector. This is the opposite tendency from that for the tangential detector.

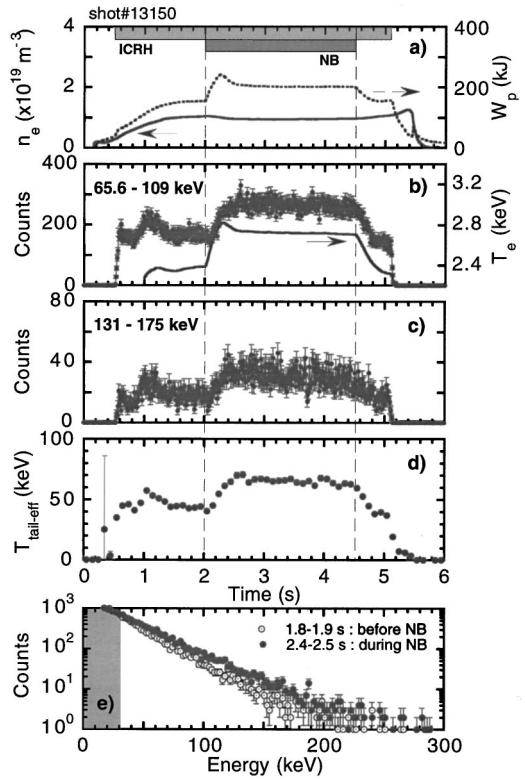

FIG. 5. Wave forms of ICRF-heated discharge with NBI in LHD, (a) n_e and W_p, (b) neutral particle flux and T_e, (c) neutral particle flux for higher energy range, (d) effective tail temperature with taking into account of charge exchange process; $H^+ + He^0 \rightarrow H^0 + He^+$, (e) energy distribution before/during NBI. B_t and R_{ax} were 2.75 T and 3.6 m, respectively. The energetic ion tail grows further during NBI.

2. Energetic ion orbit

The perpendicular NDD measures fast particles having a pitch angle of 85°–105° in R_{ax} of 3.6 m (see Fig. 1). The orbit calculation shows that particles coming from the core region are so called blocked particles. They tend to localize in the small R side of horizontally elongated cross section. Particles coming from relatively peripheral regions have helically trapped orbits. A typical orbit of helically trapped ions detected by the NDD is shown in Fig. 6. Helically trapped ions rotate poloidally due to ion ∇B drift and move toroidally along the minimum magnetic field strength of the helical ripple well. Blocked/helically trapped boundary exists at $z \approx \pm 0.3$ m ($r/a \approx 0.4$). In the third cycle of LHD, ICRF heating experiment were mostly done in B_t of 2.75 T and R_{ax} of 3.6 m. In this configuration, resonance layer of ICRF is located at relatively peripheral region, r/a of 0.5–1.0,[12] therefore, ICRF-accelerated protons we detect are supposed to be helically trapped protons.

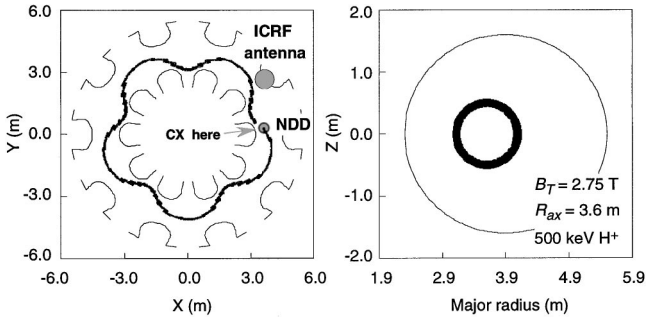

FIG. 6. Orbit of an energetic ion reaching the NDD. The NDD set on a perpendicular port detects well confined helically trapped protons during ICRF heating. B_t and R_{ax} were 2.75 T and 3.6 m, respectively.

IV. SUMMARY

Very compact solid state NPA: NDDs have been employed to measure the energy distribution of CX fast neutral particles in LHD. Energy spectra of ctr.-going beam ions and ICRF-produced energetic ions have been successfully measured by means of the NDDs and the NDDs provided various information related to energetic ion behavior in LHD, i.e., beam ion transport and energetic ion tail formation due to ICRF heating. The performance of the NDD and its good applicability to hydrogen and helium discharges of LHD were well demonstrated throughout this experiment. As a next step, poloidally aligned multichord measurements of CX fast neutrals are being planned.

ACKNOWLEDGMENTS

The authors wish to thank Professor T. Watari, Dr. R. Kumazawa, and Dr. T. Seki for useful discussion. One of the authors (M.I.) wishes to express his gratitude to Professor M. Fujiwara and Professor K. Matsuoka for their continual encouragement.

[1] R. J. Goldston, Nucl. Fusion **15**, 651 (1975).
[2] R. Kaita *et al.*, Nucl. Fusion **26**, 863 (1986).
[3] K. McGuire *et al.*, Phys. Rev. Lett. **50**, 891 (1983).
[4] R. J. Goldston, R. Kaita, P. Beiersdorfer, G. Gammel, D. L. Herndin, D. C. McCune, and D. D. Meyerhofer, Nucl. Fusion **27**, 921 (1987).
[5] R. Kaita, R. B. White, A. W. Morris, E. D. Fredrickson, K. G. McGuire, S. S. Medley, T. J. Murphy, and S. D. Scott, Phys. Fluids B **2**, 1584 (1990).
[6] M. P. Petrov, R. Bell, R. V. Bundy, N. N. Gorelenkov, S. S. Medley, R. B. White, and S. J. Zweben, Phys. Plasmas **6**, 2430 (1999).
[7] A. V. Krasilnikov, S. S. Medley, N. N. Gorelenko, R. V. Bundy, D. S. Darrow, and A. L. Roquemore, Nucl. Fusion **39**, 1111 (1999).
[8] O. Motojima *et al.*, Phys. Plasmas **6**, 1843 (1999).
[9] A. V. Krasilnikov, J. Kaneko, M. Isobe, F. Maekawa, and T. Nishitani, Rev. Sci. Instrum. **68**, 1720 (1997).
[10] A. V. Krasilnikov *et al.*, J. Plasma Fusion Res. **75**, 967 (1999).
[11] S. Murakami *et al.*, Proceedings of 6th IAEA TCM on Energetic Particles in Magnetic Confinement Systems, Naka, Japan, JAERI-Conf. 2000-04, pp 97–100.
[12] T. Seki *et al.*, Proceedings of 27th EPS Conference on Controlled Fusion and Plasma Physics (P1.104), Budapest, 2000.